

Variations on the CSC model

Ives Rey-Otero, Jeremias Sulam, Michael Elad

Abstract—Over the past decade, the celebrated sparse representation model has achieved impressive results in various signal and image processing tasks. A convolutional version of this model, termed convolutional sparse coding (CSC), has been recently reintroduced and extensively studied. CSC brings a natural remedy to the limitation of typical sparse enforcing approaches of handling global and high-dimensional signals by local, patch-based, processing. While the classic field of sparse representations has been able to cater for the diverse challenges of different signal processing tasks by considering a wide range of problem formulations, almost all available algorithms that deploy the CSC model consider the same $\ell_1 - \ell_2$ problem form. As we argue in this paper, this CSC pursuit formulation is also too restrictive as it fails to explicitly exploit some local characteristics of the signal. This work expands the range of formulations for the CSC model by proposing two convex alternatives that merge global norms with local penalties and constraints. The main contribution of this work is the derivation of efficient and provably converging algorithms to solve these new sparse coding formulations.

Index Terms—sparse representation, convolutional sparse coding, parallel proximal algorithm, convex optimization.

I. INTRODUCTION

The sparse representation model [1] is a central tool for a wide range of inverse problems in image processing, such as denoising [2], [3], super-resolution [4], [5], image deblurring [6], [7] and more. This model assumes that natural signals can be represented as a sparse linear combination of a few columns, called atoms, taken from a matrix called dictionary. The problem of recovering the sparse decomposition of a given signal over a (typically overcomplete) dictionary is called *sparse coding* or pursuit. Such an inverse problem is usually formulated as an optimization objective seeking to minimize the ℓ_0 pseudo-norm, or its convex relaxation, the ℓ_1 -norm, while allowing for a *good*¹ signal reconstruction. An effective deployment of the sparse representation model calls for the identification of a dictionary that suites the data treated. This is known as the *dictionary learning* problem, of finding the best sparsifying dictionary that fits a large set of signal examples [8], [9].

Alas, when it comes to the need to process global high-dimensional signals (e.g., complete images), the sparse representation model hits strong barriers. Dictionary learning is completely intractable in such cases due to its too high memory and computational requirements. In addition, the global pursuit fails to grasp local varying behaviors in the signal, thus leading to inferior treatment of the overall data. Because of these reasons, it has become a common practice to split the global signal into small overlapping blocks, or

patches, identify the dictionary that best models these patches, and then sparse code and reconstruct each of these blocks independently before averaging them back into a global signal [2]. Although practical and effective [10], this patch-based strategy is inherently limited since it does not account for the natural dependencies that exist between adjacent or overlapping patches, and therefore it cannot ensure a coherent reconstruction of the global signal [11], [12].

This limitation of the patch-based strategy has been tackled in two ways. One way maintains the patch-based strategy while extending it by modifying the objective so as to bridge the gap between local prior and global reconstruction. This is achieved either by taking into account the self-similarities of natural images [7], [3], by exploiting their multi-scale nature [12], [13], [14], or by explicitly requiring the reconstructed global signal to be consistent with the local prior [15], [11]. The second way consists in dropping the heuristic patch-based strategy altogether in favor of global, yet computationally tractable and locally-aware, models. Such is the case of the CSC [16], [17], [18], allowing the pursuit to be performed directly on the global signal by imposing a specific banded convolutional structure on the global dictionary. This implies, naturally, that the signal of interest is a superposition of a few local atoms shifted to different positions. And so, while the CSC is a global model, it has patch-based flavor to it and in addition, learning its dictionary is within reach [19].

Recent years have seen a renewed interest in the CSC model, including a thorough theoretical analysis along with new pursuit and dictionary learning algorithms for it, and its deployment to problems such as image inpainting, super-resolution, dynamic range imaging, and pattern classification [19], [20], [21], [22], [23], [24], [25]. Nevertheless, the research activity on the CSC model is still in its infancy. In particular, while the classic sparse representation model has assembled an extensive toolbox of problem formulations, diverse sparsity promoting penalty functions along with countless pursuit algorithms (with greedy, relaxation and Bayesian alternatives), most pursuit approaches to recover the CSC representation Γ from a global signal X and a convolutional dictionary D rely on minimizing the same $\ell_2 - \ell_1$ objective, namely

$$\underset{\Gamma}{\text{minimize}} \frac{1}{2} \|X - D\Gamma\|_2^2 + \lambda \|\Gamma\|_1, \quad (1)$$

where λ is a Lagrangian parameter. As we show in this work, this problem formulation is too restrictive and dull. Indeed, both terms in this formulation, the ℓ_2 reconstruction term and the ℓ_1 sparsity promoting penalty, are global quantities - as is the scalar Lagrangian parameter λ that controls the trade-off between them. This contrasts with state-of-the-art patch-based methods where sparsity is controlled locally, typically through a per-patch constraint on the maximum number of non-zeros or

All authors are with the Computer Science Department, Technion - Israel Institute of Technology

¹The desired representation accuracy, or fitting, is problem dependent and it varies for different applications.

on the *maximal allowed patch error* [2]. While one would hope for the CSC pursuit to optimally scatter non-zero coefficients in a way that best serves the signal, we unfortunately observe that this not to be the case in practice. Instead, solutions to the above problem typically exhibit sparsity patterns that have little relation with the signal local complexity. This calls for alternative problem formulations where local sparsity and local representation errors are explicitly taken into account in the global model.

An additional motivation for an alternative formulation of the CSC pursuit stems from the findings of [26], which is the first work to derive a theoretical analysis framework for the CSC model. In order to leverage the convolutional structure in this pursuit problem, the authors in [26] advocate for a new notion of local sparsity. In particular, they provide recovery and stability guarantees conditioned on the sparsity of each representation portion responsible for encoding individual patches, as opposed to the traditional global ℓ_0 norm. The CSC pursuit formulations proposed in the present work aim at explicitly controlling the sparsity level in these portions of the representation vectors, called stripes. The first formulation employs the $\ell_{1,\infty}$ norm as the sparsity promoting function, providing a convex relaxation of the $\ell_{0,\infty}$ pseudo-norm that was introduced in [26] and explored further in [27], [28]. The second formulation controls the sparsity of the stripes by considering the maximum reconstruction error on each patch simultaneously, via an $\ell_{2,\infty}$ norm. Such an approach is motivated by patch averaging techniques that have been successfully deployed for denoising and other inverse problems [2], [10]. We derive, for each of these two formulations, simple, efficient, and provably converging algorithms.

The remainder of the paper is organized as follows. Section II reviews common notations and definitions for the CSC model. Section III examines the behavior of the classic $\ell_2 - \ell_1$, in particular its tendency to overuse simple atoms and encode the signal by aggregation of these coarse atoms along with a spatial instability of the global representation. We then propose two alternate formulations, the $\ell_2 - \ell_{1,\infty}$ and $\ell_{2,\infty} - \ell_1$ in Section IV and Section V, respectively. Both sections focus on the derivation of algorithms to solve the respective formulations along with experiments to illustrate their behavior and performance. Section VI contains a final discussion.

II. CONVOLUTIONAL SPARSE CODING

This work uses the terminology first introduced in [26]. The CSC model assumes that an image can be decomposed as $X = D\Gamma$. An image of size $H \times W$ is represented in its vectorized form as a vector X of length $N = HW$ and the corresponding global convolutional dictionary D is of size $N \times Nm$. D is built as the concatenation of m (block-) circulant matrices of size $N \times N$, each representing one convolution. These convolutions employ small support filters of size $n \times n$, thus causing the above-mentioned circulant matrices to be narrowly banded. Another way to describe D is by combining all the shifted versions of a local dictionary $D_l \in \mathbb{R}^{n^2 \times m}$ composed of the m vectorized 2D filters. Such

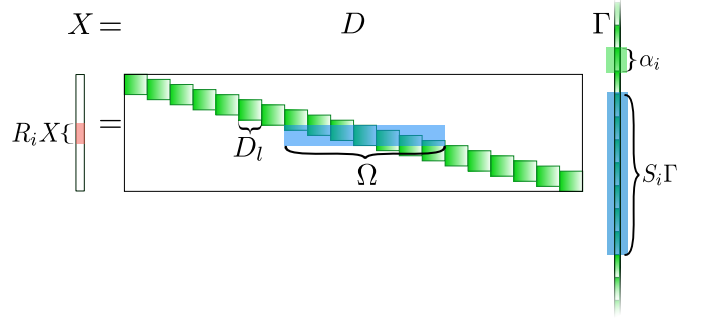


Fig. 1. Illustration of the CSC model for the 1D case. At the global scale, the image X can be decomposed into the product of the global convolutional dictionary D and a global sparse representation Γ . At the patch scale, the patch $R_i X$ can be decomposed into the product of the stripe dictionary Ω and the stripe representation vector $S_i \Gamma$.

construction is best illustrated by expressing the global signal in terms of the local dictionary, $X = \sum_{i=1}^N R_i^T D_l \alpha_i$, where R_i^T is the operator that positions the patch $D_l \alpha_i$ in the i^{th} location and pads the rest of the entries with zeros. The quantity $D_l \alpha_i$ is called a slice, with α_i being the portion of the sparse representation vector Γ , called needle, that encodes the slice. It is important to stress that slices are not patches but rather simpler components that are combined to form patches.

To better understand which parts of the dictionary D and of the sparse vector Γ represent an isolated patch, it is convenient to consider the patch extraction operator R_i and apply it to the system of equations $X = D\Gamma$. This yields the system $R_i X = R_i D \Gamma$ consisting of the n^2 rows relating to the patch pixels. Due to the banded structure of D , the extracted rows $R_i D$ contain only a subset of $(2n - 1)^2 m$ columns that are not trivially zeros. Denoting by S_i^T the operator that extracts such columns and rewriting our system of equations as $R_i X = R_i D S_i^T S_i \Gamma$ make two interesting entities come to light. The first is the vector $S_i \Gamma$, a subset of $(2n - 1)^2 m$ coefficients of Γ called the *stripe* that entirely encodes the patch $R_i X$. The second entity is the sub-matrix $\Omega = R_i D S_i^T \in \mathbb{R}^{n^2 \times (2n-1)^2 m}$, called the *stripe dictionary*, which multiplies the stripe vector $S_i \Gamma$ to reconstruct the patch. Figure 1 summarizes these definitions and notations, employed in the remainder of the paper.

III. THE NEED FOR STRUCTURED SPARSITY

To illustrate the problematic behavior of the CSC model in its most common formulation, we examine the structure obtained in the global representation vector in the following experiment. A natural image X is sparse coded using the $\ell_1 - \ell_2$ formulation², resulting in the decomposition $D\Gamma_{\text{CSC}}$. The local dictionary considered, D_l , is the DCT dictionary ($n = 8, m = 64$) and λ is set so as to reach a reconstruction error of 30 dB. For comparison, fully-overlapping patches of the same image are sparse coded individually using the Orthogonal Matching Pursuit (OMP) with the same local

²The $\ell_1 - \ell_2$ minimization is carried out using the slice-based algorithm proposed in [29].

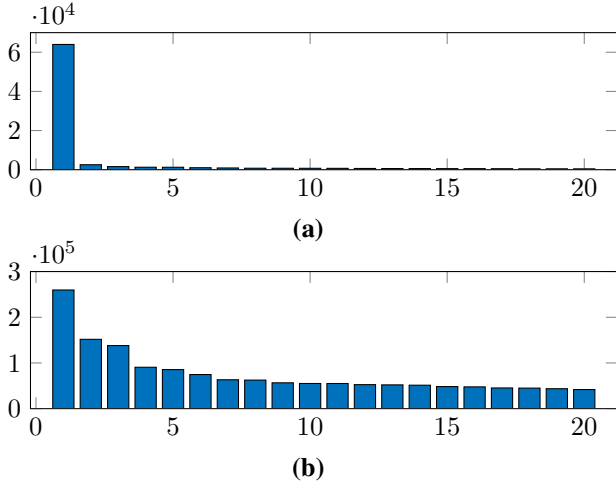


Fig. 2. Representation test for the image *barbara*. Number of non-zero coefficients for each of the 20 most commonly used atoms in each representation. **(a)** CSC $\ell_1 - \ell_2$ formulation **(b)** sparse coding every patch individually via OMP. The sparsity level in both representations is set so as to reach a reconstruction error of 30dB. In both cases, the most popular atom is the DC component. The $\ell_1 - \ell_2$ CSC formulation leads to one atom being used predominantly. Since each patch is reconstructed independently, the patch-based reconstruction leads to a denser global representation and uses diverse local atoms.

dictionary. The error threshold in the OMP is set so as to achieve a representation error of 30 dB after patch-averaging, so as to match the CSC experiment. This results in a set of needles, one per each patch, and these can be concatenated into a global sparse representation Γ_{OMP} that has the same length and structure as Γ_{CSC} .

Figures 2 **(a)** and **(b)** depict how often the first 20 atoms in the local dictionary are used in Γ_{CSC} and Γ_{OMP} respectively. In the CSC representation vector, one atom is predominantly used, namely the DC atom. In fact, most of the needles in Γ_{CSC} contain at most only one active atom, and many of them (about 70%) remain completely empty. Note that while the OMP algorithm in the patch-based approach encodes the patches using the local dictionary atoms alone, the CSC pursuit encodes the entire image using the atoms as well as their shifts. This allows fewer local atoms to be used in the CSC representation. Indeed, the system of equations $X = D\Gamma$ admits an infinite number of solutions even with a local dictionary D_l containing as few as two atoms, which would be, on the other hand, insufficient to reliably reconstruct individual patches.

What these plots show in fact is that, in the CSC model, the juxtaposition of the simplest atoms shifted at different locations accounts for most of its expressiveness. This tendency leads to a series of problems. On one hand, this is of importance for any dictionary learning algorithm that builds on the $\ell_1 - \ell_2$ formulation, since the predominant use of one filter prevents most atoms from being properly updated and learned.

Another tendency of the CSC model we would like to expose is the fact that the global representation obtained is spatially unstable. By putting too much emphasis on the spatial arrangement of slices, the sparse representation at one point

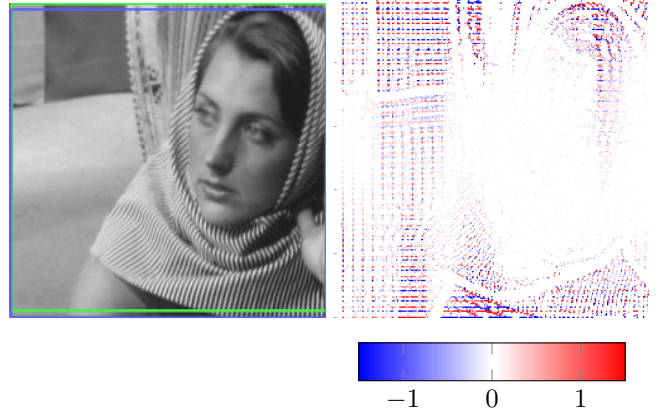


Fig. 3. Spatial instability of the CSC sparse representation. **(a)** We consider two crops setups (in green and blue) only differing by a vertical shift of 4 pixels. We sparse code each sub-image with the convolutional dictionary based on the DCT. **(b)** Sparsity difference: each pixel in the figure corresponds to the difference between the ℓ_1 -norm of the needles in each representation (after shifting back the representation by 4 pixels so as to consider the needles that are in both representations). Note that on smooth regions, representation is spatially sparse and follows a grid pattern. The $\ell_1 - \ell_2$ formulation leads to juxtaposition of slices, whose spatial arrangement is sensitive to the smallest distant variations of the signal.

of the image is overly affected by a distant structure in the image – as happens, for example, with the image borders. To demonstrate this, let us consider two image crops shifted from one another by a few pixels. The impact of the border location on the spatial distribution of non-zero coefficients is illustrated in Figure 3, which shows the difference between the respective sparsity maps (with proper compensation of the shift). Oddly, the global distribution of atoms in the image is globally affected most noticeably in smooth regions of the image.

Note that it is common in practice to deploy the CSC model not directly on the image itself but rather after applying a local mean subtraction and contrast normalization of the signal. This has the effect of mitigating, to some extent, the spatial instability to large distance interaction by breaking the connections between distant structure. However, this does not prevent the inherent tendency of the $\ell_1 - \ell_2$ global formulation to use too few atoms and compensating for this by aggregating overlapping shifts. We will see that by anchoring the CSC pursuit locally, as in the proposed alternate formulations, it is possible to get hold of such tendency.

IV. THE $\ell_2 - \ell_{1,\infty}$ CSC FORMULATION

The first alternate formulation that we explore drops the global ℓ_1 as a sparsity promoting penalty and uses instead a mixed norm function, adding an explicit and local control of sparsity. This is motivated by the work in [26], whose analysis centers around a new notion of local sparsity, the $\ell_{0,\infty}$. This measure, instead of quantifying the total number of non-zeros in a vector, reports the ℓ_0 norm of the *densest* stripe:

$$\|\Gamma\|_{0,\infty} = \max_i \|S_i \Gamma\|_0. \quad (2)$$

Such a localized norm is a somewhat more appropriate measure of sparsity in the convolutional setting, since with it one

is able to significantly improve on the theoretical guarantees for the CSC model [26]. Although that work established that the $\ell_2 - \ell_1$ formulation approximates the solution to an $\ell_{0,\infty}$ problem, it also conjectured that further improvement could be achieved by considering a new $\ell_{1,\infty}$ -norm. This norm, defined as $\|\Gamma\|_{1,\infty} = \max_i \|S_i \Gamma\|_1$, will be the center of our current discussion: the $\ell_2 - \ell_{1,\infty}$ formulation,

$$\min_{\Gamma} \frac{1}{2} \|X - D\Gamma\|_2^2 + \lambda \|\Gamma\|_{1,\infty}. \quad (3)$$

The $\ell_{1,\infty}$ is nothing but a mixed norm on the global representation Γ . Mixed-norms have been commonly used in signal processing to promote various types of structure in the sparsity pattern [30]. In the context of the CSC model, using this mixed norm is expected to promote a distribution of non-zero coefficients that makes use of more diverse local atoms and is less affected by the global attributes of the image.

This formulation, in fact, first appeared in the work of [28], which proposed a global ADMM formulation to iteratively minimize the loss in Equation (3). Unfortunately, one of the steps in their proposed iterative process requires of yet another ADMM solver, resulting in a generally inefficient algorithm. The complexity of this approach is aggravated by the need of a multi-block ADMM, which requires careful parameter tuning and does not enjoy the convergence properties of the standard ADMM.

A. The proposed algorithm

Recalling the $\ell_2 - \ell_{1,\infty}$ formulation in Equation (3), consider N splitting variables $\{\gamma_i\}_{i=1}^N$, so as to rewrite the problem equivalently as

$$\begin{aligned} \text{minimize}_{\Gamma, \{\gamma_i\}} \quad & \frac{1}{2} \|Y - D\Gamma\|_2^2 + \lambda \max_i \|\gamma_i\|_1 \\ \text{subject to} \quad & \forall i, \gamma_i = S_i \Gamma. \end{aligned} \quad (4)$$

This constrained minimization problem is handled by considering its augmented Lagrangian:

$$\begin{aligned} \text{minimize}_{\Gamma, \{\gamma_i\}, \{u_i\}} \quad & \frac{1}{2} \|Y - D\Gamma\|_2^2 + \lambda \max_i \|\gamma_i\|_1 \\ & + \frac{\rho}{2} \sum_i \|\gamma_i - S_i \Gamma + u_i\|_2^2, \end{aligned} \quad (5)$$

where $\{u_i\}_{i=1}^N$ denote the scaled dual-variables associated with each equality constraint $\gamma_i = S_i \Gamma$. The ADMM algorithm [31] minimizes this augmented Lagrangian by alternatively updating the variable Γ and the set of splitting variables $\{\gamma_i\}_{i=1}^N$. Formally, an iteration of the ADMM algorithm consists of the following steps:

$$\Gamma^{(k)} := \arg \min_{\Gamma} \frac{1}{2} \|Y - D\Gamma\|_2^2 + \frac{\rho}{2} \sum_i \|\gamma_i^{(k-1)} - S_i \Gamma + u_i^{(k-1)}\|_2^2. \quad (6)$$

$$\{\gamma_i^{(k)}\} := \arg \min_{\{\gamma_i\}} \lambda \max_i \|\gamma_i\|_1 + \frac{\rho}{2} \sum_i \|\gamma_i - S_i \Gamma^{(k)} + u_i^{(k-1)}\|_2^2. \quad (7)$$

$$u_i^{(k)} := u_i^{(k-1)} + \gamma_i^{(k)} - S_i \Gamma^{(k)}. \quad (8)$$

The update of Γ in Equation (6) is straightforward, as it is a least-square minimization that boils down to solving the linear system of equations

$$\left(D^T D + \rho \sum_i S_i^T S_i \right) \Gamma = D^T Y + \rho \sum_i S_i^T (\gamma_i + u_i). \quad (9)$$

Bearing in mind that fast (possibly GPU) implementations are available for the convolution D^T and the transpose convolution D , and using the fact that $\sum_i S_i^T S_i = (2n-1)I$, this *regularized* least-square minimization can be carried out efficiently and reliably via a few iterations of the conjugate gradient method [32].

The updates of the variables $\{\gamma_i\}_{i=1}^N$ in Equation (7) are seemingly more complicated, due to the max operation between the different stripes and the fact that they overlap. To make it more manageable, we cast the Problem (7) in epigraph form as

$$\begin{aligned} \text{minimize}_{\{\gamma_i\}, t} \quad & \lambda t + \frac{\rho}{2} \sum_i \|\gamma_i - S_i \Gamma^{(k+1)} + u_i^{(k)}\|_2^2, \\ \text{subject to} \quad & \forall i, \|\gamma_i\|_1 \leq t. \end{aligned} \quad (10)$$

Here, the initial problem with variables $\{\gamma_i\}_{i=1}^N$ has just been replaced with an equivalent minimization over variables $\{\gamma_i\}_{i=1}^N$ and t . Note that, for a fixed value of variable t , this new objective in Equation (10) is now separable in the variables $\{\gamma_i\}_{i=1}^N$. More precisely, it can be broken down into N separate minimization problems

$$\begin{aligned} \bar{\gamma}_i(t) := \arg \min_{\gamma_i} \quad & \|\gamma_i - S_i \Gamma^{(k)} + u_i^{(k-1)}\|_2^2, \\ \text{subject to} \quad & \|\gamma_i\|_1 \leq t. \end{aligned} \quad (11)$$

Each of these is simply a projection onto the ℓ_1 -ball [33] that can be performed via the shrinkage operator³:

$$\bar{\gamma}_i(t) = \mathcal{S}_{\lambda^*} \left(S_i \Gamma^{(k)} - u_i^{(k-1)} \right), \quad (12)$$

where the shrinkage parameter λ^* can be efficiently estimated by sorting the vector's coefficients and computing over them a cumulative sum (see [33] for details).

In this way, solving the initial problem (7) boils down to finding the optimal t leading to the minimum of the objective, namely $\{\gamma_i^{(k)}\}_{i=1}^N = \{\bar{\gamma}_i(t^*)\}_{i=1}^N$ with

$$t^* := \arg \min_t \left(\lambda t + \sum_i \|\bar{\gamma}_i(t) - S_i \Gamma^{(k)} + u_i^{(k-1)}\|_2^2 \right). \quad (13)$$

As a sum of an affine function and squared distances to the ℓ_1 ball of radius t , the previous objective is a convex function of t . Indeed, the distance to the ℓ_1 ball is a convex function of the radius t (see Proposition 1 in Appendix A). and it can therefore be minimized efficiently via a simple binary-search.

This simple algorithm, by not involving an over-sensitive Lagrange multiplier setting, and by enjoying the convergence properties of the standard ADMM compares favorably with the method described in [28].

³ $\mathcal{S}_{\lambda}(\mathbf{x})$ denotes the shrinkage operator, formally $\mathcal{S}_{\lambda}(\mathbf{x}) = \text{sign}(\mathbf{x}) \odot \max(|\mathbf{x}| - \lambda, 0)$, with \odot denoting the element-wise product.

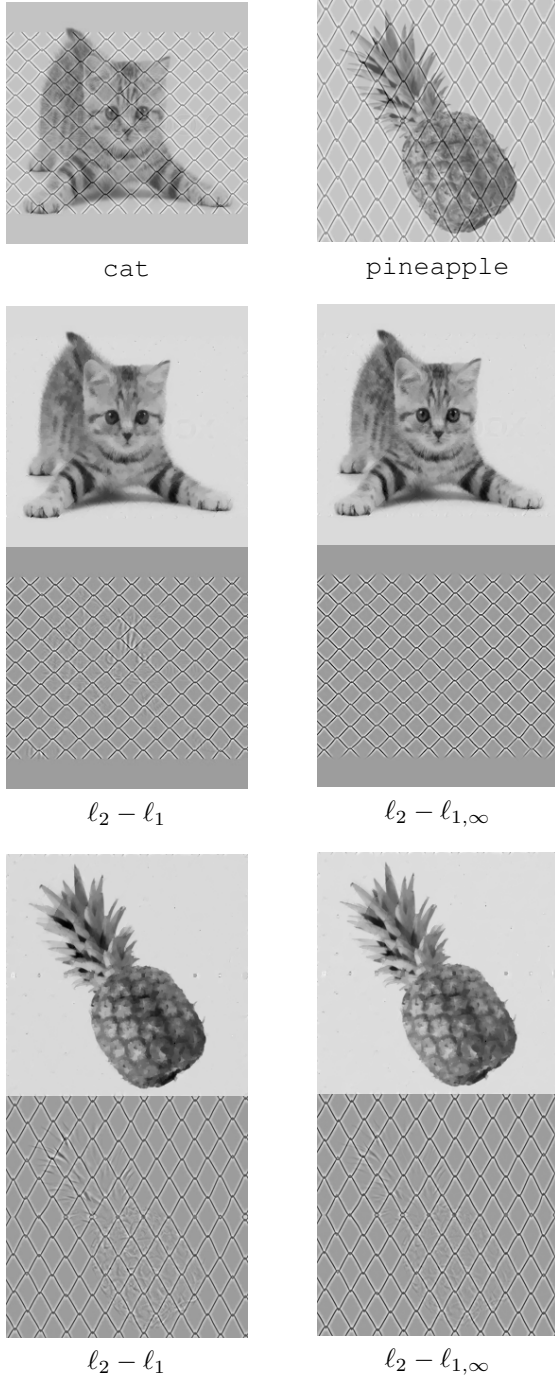


Fig. 4. Noiseless texture-cartoon separation. Comparing the $\ell_2 - \ell_{1,\infty}$ and $\ell_2 - \ell_1$ formulations. The input images consist of the test image `cat` and `pineapple`.

B. Experiments

We illustrate the $\ell_2 - \ell_{1,\infty}$ formulation on the texture-cartoon separation task. This problem consists in decomposing an input image X into a piecewise smooth component (cartoon) X_c and a texture component X_t such that $X = X_c + X_t$. The typical prior for the cartoon component X_c is based on the total variation norm, denoted $\|X_c\|_{\text{TV}}$, which penalizes oscillations. In addition, we propose to assume that the texture component X_t admits a decomposition $X_t = D_t \Gamma$ where D_t is a convolutional texture dictionary and Γ is the solution of the

$\ell_2 - \ell_{1,\infty}$ CSC formulation. Under these assumptions, the task of texture and cartoon separation boils down to a minimization problem over three variables: the cartoon component X_c , the CSC representation Γ and a convolutional texture dictionary D_t , namely

$$\underset{\Gamma, D_t, X_c}{\text{minimize}} \frac{1}{2} \|X - D_t \Gamma - X_c\|_2^2 + \lambda \|\Gamma\|_{1,\infty} + \zeta \|X_c\|_{\text{TV}}, \quad (14)$$

with parameter ζ controlling the level of TV regularization penalizing oscillations in X_c . Such minimization is carried out iteratively in a block-coordinated manner until convergence. Each iteration consists of the three following steps:

$$X_c^{(k+1)} := \arg \min_{X_c} \frac{1}{2} \|X - D_t^{(k)} \Gamma^{(k)} - X_c\|_2^2 + \zeta \|X_c\|_{\text{TV}} \quad (15)$$

$$\Gamma^{(k+1)} := \arg \min_{\Gamma} \frac{1}{2} \|X - D_t^{(k)} \Gamma - X_c^{(k+1)}\|_2^2 + \lambda \|\Gamma\|_{1,\infty} \quad (16)$$

$$D_t^{(k+1)} := \arg \min_{D_t} \frac{1}{2} \|X - D_t \Gamma^{(k+1)} - X_c^{(k+1)}\|_2^2. \quad (17)$$

A TV denoiser⁴ is used to solve Problem (15) while Problem (16) relies on our $\ell_2 - \ell_{1,\infty}$ solver. For the dictionary update, one option is to use a standard patch-based dictionary learning such as K-SVD using overlapping patches as training sets and the needles of the current Γ estimate. However this would not be consistent with the CSC model. Indeed, the patch would then be assumed to stem from the local dictionary alone, disregarding all the contributions of shifted atoms to its reconstruction. We adopt instead a more coherent alternative that was recently proposed in [27] in which standard dictionary update procedures are adapted to a convolutional setting and carried out via conjugate gradient descent [32] in conjunction with fast convolution computations. The proposed method is applied to the test images `cat` and `pineapple`, the results of our method are shown in Figure 4 along with the results from the $\ell_1 - \ell_2$ based method in [29]

V. THE $\ell_{2,\infty} - \ell_1$ CSC FORMULATION

We move on to consider our second formulation, of explicitly incorporating a local control on the CSC model. This is inspired by the patch-based strategy for image denoising and other inverse problems. Recall that patch-based sparse denoising methods [2], [10] control the sparsity level on each patch by upper-bounding the patch reconstruction error. We will borrow such an idea, and translate it into the convolutional setting.

For a noisy image Y , patch methods rely on a global objective of the form

$$\underset{\{\alpha_i\}, X}{\text{minimize}} \frac{\lambda}{2} \|X - Y\|_2^2 + \sum_i \|\beta_i\|_0 \quad (18)$$

$$\text{subject to} \quad \forall i, \|D_i \beta_i - R_i X\|_2^2 \leq T,$$

where β_i is the sparse vector for the patch $R_i X$ and the upper-bound T over the patch reconstruction error is typically

⁴The TV denoiser used here is the publicly available implementation of [34].

set to $Cn^2\sigma_{\text{noise}}^2$, the assumed patch noise level (up to a multiplicative constant). This is typically solved via a block-coordinate descent algorithm, which means first initializing $X = Y$ and seeking the sparsest α_i for each patch via the set of local problems

$$\begin{aligned} & \underset{\beta_i}{\text{minimize}} && \|\beta_i\|_0 \\ & \text{subject to} && \|D_i\beta_i - R_iY\|_2^2 \leq T, \end{aligned} \quad (19)$$

which yields a reconstruction for each overlapping patch and, in turn, an intermediary global reconstruction $\frac{1}{n^2} \sum_i R_i^T D_L \beta_i$. While state-of-the-art methods typically consider approximate solutions through greedy pursuit algorithms, it is also possible to consider an ℓ_1 relaxation of the same sparse coding problem. We will employ the latter option in order to benefit from the resulting convexity of the problem.

The second stage of the block-coordinate descent algorithm consists in updating the estimate of X , the restored image, by solving the least-square problem in closed form [2] according to:

$$X = \left(\lambda I + \sum_i R_i^T R_i \right)^{-1} \left(\lambda Y + \sum_i R_i^T D_L \beta_i \right), \quad (20)$$

essentially averaging the input signal Y with the patch-averaging estimate $\frac{1}{n^2} \sum_i R_i^T D_L \beta_i$.

In order to bring this classic approach into a convolutional setting, note that the CSC global representation Γ can be decomposed into its constituent *needles*, and so $\sum_i \|\alpha_i\|_1 = \|\Gamma\|_1$. Recalling the definitions and notations in Section II, a patch from the reconstructed image $R_i X$ in the CSC model can be equivalently written as $R_i X = R_i D \Gamma = \Omega S_i \Gamma$. With these elements, the problem in (18) can be naturally transformed into

$$\begin{aligned} & \underset{\{\alpha_i\}, X}{\text{minimize}} && \frac{\lambda}{2} \|X - Y\|_2^2 + \|\Gamma\|_1 \\ & \text{subject to} && \forall i, \|\Omega S_i \Gamma - R_i X\|_2^2 \leq T. \end{aligned} \quad (21)$$

One might indeed adopt a similar block-coordinate descent strategy for this problem as well. After an initialization of $X = Y$, the first step considers the resulting $\ell_{2,\infty} - \ell_1$ formulation:

$$\begin{aligned} & \underset{\Gamma}{\text{minimize}} && \|\Gamma\|_1 \\ & \text{subject to} && \forall i, \|\Omega S_i \Gamma - R_i Y\|_2^2 \leq T, \end{aligned} \quad (22)$$

where the constraint on patch reconstruction considers the stripe dictionary. Again, the second stage consists in updating the estimate of X by solving the least-square problem

$$X = \left(\lambda I + \sum_i R_i^T R_i \right)^{-1} \left(\lambda Y + \sum_i R_i^T \Omega S_i \Gamma \right). \quad (23)$$

whose solution, since $\sum_i R_i^T \Omega S_i \Gamma = n^2 D \Gamma$ and since $\sum_i R_i^T R_i = n^2 I$, boils down to an average between the input image and the intermediary global reconstruction $D \Gamma$. In this manner, and similarly to the patch-averaging strategy, the trade-off between sparsity and reconstruction is controlled locally via an upper-bound on the reconstruction error of each individual patch. However, while in the original method each vector β_i encodes one patch in disregard with other

patches, now each needle α_i becomes part of various stripes $S_i \Gamma$ and therefore contributes in various patches. In other words, the classic patch-averaging approach performs these pursuit independently, whereas this convolutional counterpart will need to update all needles jointly.

In what follows, we show that this seemingly complex problem can in fact be addressed by using traditional ℓ_1 solvers such as the Fast Iterative Shrinkage-Thresholding Algorithm (FISTA) [35] in conjunction with the Parallel Proximal Algorithm (PPXA).

A. Proposed algorithm

PPXA is a generic convex optimization algorithm introduced by Combettes and Pesquet [36], [37] that extends the Douglas-Rachford algorithm and aims to minimize an objective of the form

$$\underset{x}{\text{minimize}} \sum_i^N f_i(x), \quad (24)$$

where each f_i is a convex function that admits an easy-to-compute proximal operator [38], [39]. Recall that the proximity operator $\text{prox}_{f_i}(y) : \mathbb{R}^N \rightarrow \mathbb{R}^N$ of f_i is defined by

$$\text{prox}_{f_i}(y) := \arg \min_x f_i(x) + 1/2 \|x - y\|_2^2. \quad (25)$$

In our context, PPXA offers a way to manage the explicit use of overlapping stripes. Indeed, by encapsulating each inequality constraint into its corresponding indicator function, the objective in Equation (22) can be recast as a sum, namely

$$\underset{\Gamma}{\text{minimize}} \sum_{i=1}^N \left(\frac{1}{N} \|\Gamma\|_1 + \mathcal{I}_{\{\|\Omega S_i \Gamma - R_i Y\|_2^2 \leq T\}} \right), \quad (26)$$

where $\mathcal{I}_{\{\|\Omega S_i \Gamma - R_i Y\|_2^2 \leq T\}}$ denotes the indicator function⁵ on the constraint feasibility set. The successful deployment of the PPXA algorithm for this problem depends on our ability to compute, for each patch, the proximal operator

$$\begin{aligned} \text{prox}_{f_i}(\Gamma) := \arg \min_{\hat{\Gamma}} & \|\hat{\Gamma}\|_1 + \frac{1}{2N\mu} \|\Gamma - \hat{\Gamma}\|_2^2 \\ & + \mathcal{I}_{\{\|\Omega S_i \hat{\Gamma} - R_i Y\|_2^2 \leq T\}}, \end{aligned} \quad (27)$$

with parameter μ scaling the least-square term. The solution to the above problem is also the solution to a Lagrangian

$$\arg \min_{\hat{\Gamma}} \|\hat{\Gamma}\|_1 + \frac{1}{2N\mu} \|\Gamma - \hat{\Gamma}\|_2^2 + \lambda_i^* \|R_i(D\hat{\Gamma} - Y)\|_2^2, \quad (28)$$

in which the Lagrange multiplier is set to an optimal value λ_i^* : the *smallest* Lagrange multiplier such that the inequality constraint is satisfied. Observe that, while transitioning from Equation (27) to Equation (28), we moved from Ω to D , in order to pose the algorithm w.r.t. the global dictionary. Fortunately, for a given Lagrangian multiplier λ_i , such objective can be efficiently minimized by a proximal gradient method such as (ISTA) [40] or its fast version FISTA [35]. Indeed,

⁵The indicator function \mathcal{I}_S equals 0 inside the set S and ∞ elsewhere.

denoting $g_i(\hat{\Gamma}, \lambda_i) := \frac{1}{2N\mu} \|\Gamma - \hat{\Gamma}\|_2^2 + \lambda_i \|R_i(D\hat{\Gamma} - Y)\|_2^2$, ISTA and FISTA revolve around the update step

$$\hat{\Gamma}^{(k+1)} = \mathcal{S}_{t_k} \left(\hat{\Gamma}^{(k)} + t_k \frac{\partial g_i}{\partial \hat{\Gamma}}(\hat{\Gamma}^{(k)}, \lambda_i) \right), \quad (29)$$

where t_k denotes the step-size⁶. The dominant effort here is the evaluation of the gradient of g_i with respect to $\hat{\Gamma}$. This boils down to the computation of convolutions, for which fast GPU implementations are available. Running FISTA successively with warm-start initialization allows to estimate the minimizer for different values of λ_i with only few extra iterations. This allows to use a binary-search scheme to estimate the optimal Lagrange multiplier λ_i^* which in turn provides the solution to the proximal operator in Equation (27).

Armed with this procedure to compute the proximal operators, an iteration of the PPXA algorithm boils down to the following steps:

- 1) Compute the proximal operators for each patch

$$\forall i = 1 \dots N, \quad \hat{\Gamma}_i^{(l)} = \text{prox}_{f_i}(\Gamma_i^{(l)}), \quad (30)$$

following the procedure described above. The evaluations can be carried out in parallel.

- 2) Aggregate the solutions

$$\hat{\Gamma}^{(l)} = \frac{1}{N} \sum_i \hat{\Gamma}_i^{(l)}. \quad (31)$$

- 3) Update the estimate of Γ along with the auxiliary variables Γ_i

$$\forall i, \quad \Gamma_i^{(l+1)} = \Gamma_i^{(n)} + \rho_l \left(2\hat{\Gamma}^{(l)} - \Gamma^{(l)} - \hat{\Gamma}_i^{(l)} \right), \quad (32)$$

$$\Gamma^{(l+1)} = \Gamma^{(l)} + \rho_l (\hat{\Gamma}^{(l)} - \Gamma^{(l)}),$$

where ρ_l denotes the relaxation parameter⁷ on this iteration. The sequence of sparse vector estimates $\Gamma^{(l)}$ is proven to converge to the solution of the $\ell_{2,\infty} - \ell_1$ CSC problem (22) [36]. Note that using FISTA in conjunction with PPXA makes it possible to take full advantage of GPU hardware and high-level libraries for fast convolutions, in contrast with most sparse coding algorithm that operate in the Fourier domain [20], [22].

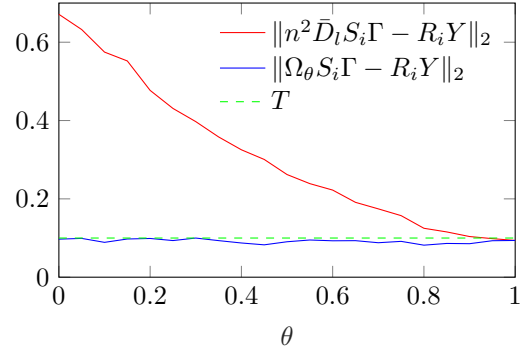
B. Extension via weighted stripe dictionary

The method described above for the $\ell_{2,\infty} - \ell_1$ formulation brings an additional level of flexibility by offering a generic way to enforce a wider range of structured sparsity. Indeed, because the proposed method splits the global pursuit into parallel pursuits on each stripe, a specific local structure can be imposed on individual stripes. This can be achieved naturally by simply weighting the columns of the stripe dictionary, so as to relatively promote or penalize the use of certain atoms. Formally this corresponds to

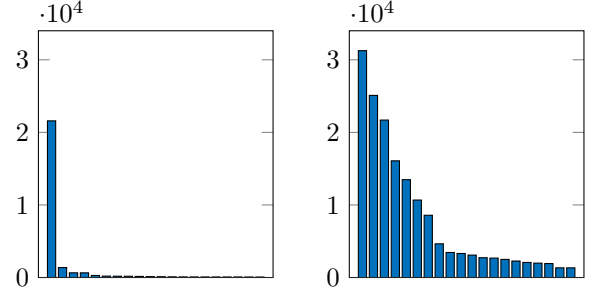
$$\begin{aligned} & \underset{\Gamma}{\text{minimize}} && \|\Gamma\|_1 \\ & \text{subject to} && \forall i, \|\Omega W_i S_i \Gamma - R_i Y\|_2^2 \leq T, \end{aligned} \quad (33)$$

⁶For convergence, the step-size t_k must satisfy $t_k \leq \frac{1}{\lambda_{\max}}$, where λ_{\max} denotes the maximum eigenvalue of ∇g_i which can be approximated efficiently via the power method.

⁷To guaranty convergence, the relaxation parameters (ρ_l) must satisfy $\sum_{l \in \mathbb{N}} \rho_l (2 - \rho_l) = +\infty$.



(a)



(b) $\theta = 0.1$

(c) $\theta = 0.8$

Fig. 5. Effect of replacing the stripe dictionary Ω with the convex combination $\Omega_\theta = (1 - \theta)\Omega + \theta n^2 \bar{D}_l$ to sparse-code the image *barbara* after local contrast normalization. (a) The average reconstruction error $\|\Omega_\theta S_i \Gamma - R_i Y\|_2$ (in blue) and the average Euclidean distance between patches and slices $\|n^2 \bar{D}_l S_i \Gamma - R_i Y\|_2$ (in red) as a function of θ . In accordance to the inequality constraint, the reconstruction error remains below the threshold T . By construction, overlapping slices must be combined to approximate patches. However, as θ increases, individual slices $n^2 \bar{D}_l S_i \Gamma$ become increasingly similar to patches. (b) and (c) Number of non-zero coefficients for each of the 20 most commonly used atoms for $\theta = 0.1$ and $\theta = 0.8$ respectively. As θ increases, more diverse local atoms are used.

where W_i denotes the weighting diagonal matrix relative to the i -th patch⁸. In the context of the proposed algorithm, this boils down to an extra weighting within each FISTA iterations.

One particularly interesting application of such strategy consists in combining the CSC and patch-averaging models. Such a combination allows for the benefits of both the global and local models, which respective performances on various tasks are increasingly well understood. From an analysis stand point, being able to examine the entire spectrum separating the CSC model and the patch-averaging approach is highly valuable, as the understand of their precise inter-relation has been of interest to the image processing community [41]. With the proposed method, such combination can be achieved via a mere re-weighting of the columns that amounts to replacing the stripe dictionary with the convex combination

$$\Omega_\theta = (1 - \theta)\Omega + \theta n^2 \bar{D}_l, \quad (34)$$

with $0 \leq \theta \leq 1$ and with \bar{D}_l denoting the local dictionary padded with zero columns. The parameter θ allows to regulate the level of patch aggregation that has been proven to be critical in denoising problems [41]. Setting $\theta = 0$ corresponds

⁸Note that to be consistent with the global CSC model, the set of matrices $\{W_i\}$ must satisfy the relation $D = \frac{1}{n^2} \sum R_i^T \Omega W_i S_i$

to the $\ell_1 - \ell_{2,\infty}$ CSC formulation above. By increasing θ , filters which locations are shifted with respect to the patch are increasingly penalized. Setting $\theta = 1$ is synonymous with the patch averaging strategy in which the reconstruction relies exclusively on D_l and none of its shifted atoms. The behavior of the resulting problem

$$\begin{aligned} & \underset{\Gamma}{\text{minimize}} && \|\Gamma\|_1 \\ & \text{subject to} && \forall i, \|\Omega_\theta S_i \Gamma - R_i Y\|_2^2 \leq T, \end{aligned} \quad (35)$$

and the structure of its solution are examined in Figure 5. Figure 5 (a) shows the average representation error $\|\Omega_\theta S_i - R_i Y\|_2$ (in blue) and the average Euclidean distance between individual slices and patches $\|n^2 \bar{D}_l S_i \Gamma - R_i Y\|$ (in red) as a functions of the parameter θ . In accordance to the inequality constraints in Problem (22), the patch reconstruction error stays below the threshold T . On the other hand, and as expected, the Euclidean distance between slices and patches is above the threshold T , as it is the combination of overlapping slices, rather than an isolated slice, that approximates the patch. However, as θ increases, the term $\Omega_\theta S_i \Gamma$ in the representation error in Problem (35) is increasingly similar to a slice $n^2 D_l \alpha$. This in turn constrains the individual slices to better approximate the corresponding patch. Additionally, the constraint affects the diversity of local atoms used in the global representation. Indeed, Figure 5 (b) and (c) show the number of non-zero coefficients for $\theta = 0.1$ and $\theta = 0.8$ respectively. Even though the formulations for $\theta = 0.1$ and $\theta = 0.8$ are both consistent with the global CSC model, the latter leads to more diverse local atoms being used. We will see next how this behavior brings additional practical benefits.

C. Experiments

We illustrate the behavior of the $\ell_{2,\infty} - \ell_1$ formulation and its weighted variant on the classic problem of image inpainting. Let us consider an image X and a diagonal binary matrix M , which masks the entries in X in which $M_{i,i} = 0$. Image inpainting is the process of filling in missing areas in an image in a realistic manner. That is, given the corrupted image $Y = MX$, the task consists in estimating the original signal X .

Estimating the original signal via the $\ell_{2,\infty} - \ell_1$ CSC requires solving the problem

$$\begin{aligned} & \underset{\Gamma}{\text{minimize}} && \|\Gamma\|_1 \\ & \text{subject to} && \forall i, \|R_i(MD\Gamma - Y)\|_2^2 \leq T_i, \end{aligned} \quad (36)$$

where the constraint on the representation accuracy incorporates the binary matrix M , and where the threshold T_i is set on a patch-by-patch basis to reflect the varying numbers of active pixels in each patch. Minimizing this objective requires only a slight modification of the algorithm described above, namely incorporating the mask into the function g_i and its gradient. The PPXA relaxation parameter is set to $\lambda_i = 1.6$ and the scaling factor in the proximal operator is set to $\mu = 100$.

Table I contains the peak signal-to-noise ratio (PSNR) on a set of publicly available standard test images. In the first block of experiments, we adopt the benchmark framework proposed

in [20]. In particular, the local contrast normalization is applied to the input image and the local dictionary is pretrained from the `fruit` dataset, using the method from [29]. The method based on the $\ell_{2,\infty} - \ell_1$ formulation outperforms the method proposed in [20] and slightly improves over the slice-based approach of [29]. The best performance are obtained in general with the weighted $\ell_{2,\infty} - \ell_1$ ($\theta = 0.8$), which formulation tends to promote an averaging of similar local estimates. Significant additional improvements are achieved when learning the local dictionary D_l from the corrupted image. The second block in Table I contains the inpainting PSNR obtained in this scenario for the sliced based method [29] and for the weighted $\ell_{2,\infty} - \ell_1$ used along the dictionary update proposed in [27]. In this context, the weighting of the stripe dictionary is particularly beneficial as it encourages more atoms to be used and therefore updated (see Figure 5).

VI. CONCLUSION

While enjoying a renewed interest in recent years, the CSC model has been almost exclusively considered in its $\ell_2 - \ell_1$ formulation. In the present work, we expanded the formulations for the CSC with two alternative formulations, namely the $\ell_2 - \ell_{1,\infty}$ and $\ell_{2,\infty} - \ell_1$ formulations in which mixed-norms, alter how the spatial distributions of non-zero coefficients are controlled. For both formulations, we derived algorithms that rely on the ADMM and PPXA algorithms. The algorithms are simple, easy to implement and can take full advantage of fast GPU implementation of the convolution operator. Their convergence naturally follows from the convergence properties of the two standard convex optimization framework they build on. We examined the performance and behavior of the proposed formulation on two image processing tasks: inpainting and cartoon texture separation. Furthermore, we showed that the $\ell_{2,\infty} - \ell_1$ formulation in particular opens the door to a wide variety of structured sparsity, that could bring additional practical benefits while still being consistent with the CSC model. An interesting example of such structured sparsity was offered in the combination of the CSC and patch-averaging models, showing that such a mixture provides improved performance. Finally, we envision that similar combinations of global and local sparse priors, within the proposed unifying framework, will allow to further benefits in several other restoration problems.

VII. ACKNOWLEDGEMENTS

The research leading to these results has received funding in part from the European Research Council under EUs 7th Framework Program, ERC under Grant 320649, and in part by Israel Science Foundation (ISF) grant no. 1770/14.

| | barbara | lena | boat | hill | house | couple | man |
|--|--------------|--------------|--------------|--------------|--------------|--------------|--------------|
| Heide et al. [20] | 11.00 | 11.77 | 10.29 | 10.37 | 10.18 | 11.99 | 11.60 |
| Papayan et al. [29] | 11.67 | 11.92 | 10.33 | 10.66 | 10.56 | 12.25 | 11.84 |
| $\ell_1 - \ell_{2,\infty}$ | 11.65 | 11.99 | 10.39 | 10.55 | 10.60 | 12.34 | 11.91 |
| weighted $\ell_1 - \ell_{2,\infty}$, | 11.78 | 12.13 | 10.58 | 10.65 | 10.62 | 12.46 | 11.98 |
| Papayan et al. [29], image specific D_l | 15.20 | 12.35 | 11.60 | 10.90 | 11.70 | 12.41 | 11.71 |
| weighted $\ell_1 - \ell_{2,\infty}$, image specific D_l | 16.11 | 12.29 | 11.93 | 11.22 | 12.13 | 13.16 | 12.05 |

TABLE I

IMAGE INPAINTING. THE $\ell_2 - \ell_1$ BASED METHOD OF [29] AND [20] ARE COMPARED TO THE PROPOSED METHODS: THE $\ell_{2,\infty} - \ell_1$ FORMULATION AND THE FORMULATION WITH A WEIGHTED STRIPE DICTIONARY. IN THE FIRST BLOCK, THE LOCAL DICTIONARY IS PRETRAINED FROM THE FRUIT DATASET USING THE METHOD FROM [29]. THE $\ell_{2,\infty}$ PRIOR IMPROVES OVER THE BEST $\ell_2 - \ell_1$ BASED METHOD FORMULATION. THE WEIGHTED STRIPE DICTIONARY Ω_θ WITH $\theta = 0.8$ BRINGS AN ADDITIONAL IMPROVEMENT IN PSNR OVER THE STANDARD $\ell_{2,\infty}$ BY PROMOTING PATCH AVERAGING. IN THE RESULT REPORTED IN THE SECOND BLOCK, THE LOCAL DICTIONARY USED IS LEARNED FROM THE CORRUPTED IMAGE. IN THIS SCENARIO, THE WEIGHTED $\ell_{2,\infty} - \ell_1$ FORMULATION WITH $\theta = 0.8$ GENERALLY OUTPERFORMS [29].

REFERENCES

- [1] Michael Elad, *Sparse and Redundant Representations - From Theory to Applications in Signal and Image Processing.*, Springer, 2010.
- [2] Michael Elad and Michal Aharon, "Image denoising via sparse and redundant representations over learned dictionaries," *IEEE Transactions on Image processing*, vol. 15, no. 12, pp. 3736–3745, 2006.
- [3] Julien Mairal, Francis Bach, Jean Ponce, Guillermo Sapiro, and Andrew Zisserman, "Non-local sparse models for image restoration," in *Computer Vision, 2009 IEEE 12th International Conference on*. IEEE, 2009, pp. 2272–2279.
- [4] Yaniv Romano, Matan Protter, and Michael Elad, "Single image interpolation via adaptive non-local sparsity-based modeling," *IEEE Transactions on Image Processing*, 2014.
- [5] Jianchao Yang, John Wright, Thomas S Huang, and Yi Ma, "Image super-resolution via sparse representation," *IEEE transactions on image processing*, vol. 19, no. 11, pp. 2861–2873, 2010.
- [6] Guoshen Yu, Guillermo Sapiro, and Stéphane Mallat, "Solving inverse problems with piecewise linear estimators: From gaussian mixture models to structured sparsity," *IEEE Transactions on Image Processing*, vol. 21, no. 5, pp. 2481–2499, 2012.
- [7] Weisheng Dong, Lei Zhang, Guangming Shi, and Xin Li, "Nonlocally centralized sparse representation for image restoration," *IEEE Transactions on Image Processing*, vol. 22, no. 4, pp. 1620–1630, 2013.
- [8] Michal Aharon, Michael Elad, and Alfred Bruckstein, "K-svd: An algorithm for designing overcomplete dictionaries for sparse representation," *IEEE Transactions on signal processing*, vol. 54, no. 11, pp. 4311–4322, 2006.
- [9] Kjersti Engan, Sven Ole Aase, and J Hakon Husoy, "Method of optimal directions for frame design," in *Acoustics, Speech, and Signal Processing, 1999. Proceedings., 1999 IEEE International Conference on*. IEEE, 1999, vol. 5, pp. 2443–2446.
- [10] Julien Mairal, Michael Elad, and Guillermo Sapiro, "Sparse representation for color image restoration," *IEEE Transactions on image processing*, vol. 17, no. 1, pp. 53–69, 2008.
- [11] Jeremias Sulam and Michael Elad, "Expected patch log likelihood with a sparse prior," in *International Workshop on Energy Minimization Methods in Computer Vision and Pattern Recognition*. Springer, 2015, pp. 99–111.
- [12] Vardan Papayan and Michael Elad, "Multi-scale patch-based image restoration," *IEEE Transactions on image processing*, vol. 25, no. 1, pp. 249–261, 2016.
- [13] Julien Mairal, Guillermo Sapiro, and Michael Elad, "Learning multiscale sparse representations for image and video restoration," *Multiscale Modeling & Simulation*, vol. 7, no. 1, pp. 214–241, 2008.
- [14] Jeremias Sulam, Boaz Ophir, and Michael Elad, "Image denoising through multi-scale learnt dictionaries," in *Image Processing (ICIP), 2014 IEEE International Conference on*. IEEE, 2014, pp. 808–812.
- [15] Daniel Zoran and Yair Weiss, "From learning models of natural image patches to whole image restoration," in *Computer Vision (ICCV), 2011 IEEE International Conference on*. IEEE, 2011, pp. 479–486.
- [16] Roger Grosse, Rajat Raina, Helen Kwong, and Andrew Y Ng, "Shift-invariant sparse coding for audio classification," *arXiv preprint arXiv:1206.5241*, 2012.
- [17] Jayaraman Thiagarajan, Karthikeyan Ramamurthy, and Andreas Spanias, "Shift-invariant sparse representation of images using learned dictionaries," in *Machine Learning for Signal Processing, 2008. MLSP 2008. IEEE Workshop on*. IEEE, 2008, pp. 145–150.
- [18] Cristian Rusu, Bogdan Dumitrescu, and Sotirios A Tsaftaris, "Explicit shift-invariant dictionary learning," *IEEE Signal Processing Letters*, vol. 21, no. 1, pp. 6–9, 2014.
- [19] Hilton Bristow, Anders Eriksson, and Simon Lucey, "Fast convolutional sparse coding," in *Proceedings of the IEEE Conference on Computer Vision and Pattern Recognition*, 2013, pp. 391–398.
- [20] Felix Heide, Wolfgang Heidrich, and Gordon Wetzstein, "Fast and flexible convolutional sparse coding," in *Proceedings of the IEEE Conference on Computer Vision and Pattern Recognition*, 2015, pp. 5135–5143.
- [21] Bailey Kong and Charless C. Fowlkes, "Fast convolutional sparse coding (fcsc)," *Department of Computer Science, University of California, Irvine, Tech. Rep.*, vol. 3, 2014.
- [22] Brendt Wohlberg, "Efficient convolutional sparse coding," in *Acoustics, Speech and Signal Processing (ICASSP), 2014 IEEE International Conference on*. IEEE, 2014, pp. 7173–7177.
- [23] Shuhang Gu, Wangmeng Zuo, Qi Xie, Deyu Meng, Xiangchu Feng, and Lei Zhang, "Convolutional sparse coding for image super-resolution," in *Proceedings of the IEEE International Conference on Computer Vision*, 2015, pp. 1823–1831.
- [24] Florence Yellin, Benjamin D. Haeffele, and René Vidal, "Blood cell detection and counting in holographic lens-free imaging by convolutional sparse dictionary learning and coding," in *Biomedical Imaging (ISBI 2017), 2017 IEEE 14th International Symposium on*. IEEE, 2017, pp. 650–653.
- [25] Ana Serrano, Felix Heide, Diego Gutierrez, Gordon Wetzstein, and Belen Masia, "Convolutional sparse coding for high dynamic range imaging," in *Computer Graphics Forum*. Wiley Online Library, 2016, vol. 35, pp. 153–163.
- [26] Vardan Papayan, Jeremias Sulam, and Michael Elad, "Working locally thinking globally: Theoretical guarantees for convolutional sparse coding," *IEEE Transactions on Signal Processing*, vol. 65, no. 21, pp. 5687–5701, 2017.
- [27] Elad Plaut and Raja Giryes, "Matching pursuit based convolutional sparse coding," in *Acoustics, Speech and Signal Processing (ICASSP), 2018 IEEE International Conference on*. IEEE, 2018, IEEE SigPort.
- [28] Brendt Wohlberg, "Convolutional sparse coding with overlapping group norms," *arXiv preprint arXiv:1708.09038*, 2017.
- [29] Vardan Papayan, Yaniv Romano, Michael Elad, and Jeremias Sulam, "Convolutional dictionary learning via local processing.," in *ICCV*, 2017, pp. 5306–5314.
- [30] Matthieu Kowalski, "Sparse regression using mixed norms," *Applied and Computational Harmonic Analysis*, vol. 27, no. 3, pp. 303–324, 2009.
- [31] Stephen Boyd, Neal Parikh, Eric Chu, Borja Peleato, Jonathan Eckstein, et al., "Distributed optimization and statistical learning via the alternating direction method of multipliers," *Foundations and Trends® in Machine Learning*, vol. 3, no. 1, pp. 1–122, 2011.
- [32] Carl T Kelley, *Iterative methods for optimization*, vol. 18, Siam, 1999.
- [33] John Duchi, Shai Shalev-Shwartz, Yoram Singer, and Tushar Chandra, "Efficient projections onto the l_1 -ball for learning in high dimensions," in *Proceedings of the 25th international conference on Machine learning*. ACM, 2008, pp. 272–279.
- [34] Stanley H Chan, Ramsin Khoshabeh, Kristofor B Gibson, Philip E Gill, and Truong Q Nguyen, "An augmented lagrangian method for total variation video restoration," *IEEE Transactions on Image Processing*, vol. 20, no. 11, pp. 3097–3111, 2011.
- [35] Amir Beck and Marc Teboulle, "A fast iterative shrinkage-thresholding

- algorithm for linear inverse problems,” *SIAM journal on imaging sciences*, vol. 2, no. 1, pp. 183–202, 2009.
- [36] Patrick L Combettes and Jean-Christophe Pesquet, “A proximal decomposition method for solving convex variational inverse problems,” *Inverse problems*, vol. 24, no. 6, pp. 065014, 2008.
- [37] Patrick L Combettes and Jean-Christophe Pesquet, “Proximal splitting methods in signal processing,” in *Fixed-point algorithms for inverse problems in science and engineering*, pp. 185–212. Springer, 2011.
- [38] Neal Parikh, Stephen Boyd, et al., “Proximal algorithms,” *Foundations and Trends® in Optimization*, vol. 1, no. 3, pp. 127–239, 2014.
- [39] Heinz H Bauschke, Patrick L Combettes, et al., *Convex analysis and monotone operator theory in Hilbert spaces*, vol. 408, Springer, 2011.
- [40] Ingrid Daubechies, Michel Defrise, and Christine De Mol, “An iterative thresholding algorithm for linear inverse problems with a sparsity constraint,” *Communications on Pure and Applied Mathematics: A Journal Issued by the Courant Institute of Mathematical Sciences*, vol. 57, no. 11, pp. 1413–1457, 2004.
- [41] Diego Carrera, Giacomo Boracchi, Alessandro Foi, and Brendt Wohlberg, “Sparse overcomplete denoising: aggregation versus global optimization,” *IEEE Signal Processing Letters*, vol. 24, no. 10, pp. 1468–1472, 2017.

APPENDIX

Proposition 1. *For a point y and the ℓ_1 -ball of radius r , $\mathcal{B}_r := \{x, \text{s.t. } \|x\|_1 \leq r\}$, the distance between y and the ball*

$$d(y, \mathcal{B}_r) := \inf \{ \|x - y\|_2, \mid x \in \mathcal{B}_r \},$$

is a convex function of the ball radius r .

Proof. From the ℓ_1 -norm triangle inequality, it comes that for any convex combination of two radii $\theta r_1 + (1 - \theta)r_2$, with $0 \leq \theta \leq 1$, we have the inclusion

$$\theta \mathcal{B}_{r_1} + (1 - \theta) \mathcal{B}_{r_2} \subset \mathcal{B}_{\theta r_1 + (1 - \theta)r_2},$$

where $\theta \mathcal{B}_{r_1}$ denotes the set of points $\{\theta x_1 \mid x_1 \in \mathcal{B}_{r_1}\}$. In particular, for the nearest points to y in \mathcal{B}_{r_1} and \mathcal{B}_{r_2} respectively, *i.e.*, for $x_1 \in \mathcal{B}_{r_1}$ such that $\|y - x_1\|_2 = d(y, \mathcal{B}_{r_1})$ and $x_2 \in \mathcal{B}_{r_2}$ such that $\|y - x_2\|_2 = d(y, \mathcal{B}_{r_2})$, we have

$$\theta x_1 + (1 - \theta)x_2 \in \mathcal{B}_{\theta r_1 + (1 - \theta)r_2},$$

and therefore

$$\|y - (\theta x_1 + (1 - \theta)x_2)\|_2 \geq d(y, \mathcal{B}_{\theta r_1 + (1 - \theta)r_2}).$$

Finally, from the Euclidean norm triangle inequality, it comes that

$$\theta d(y, \mathcal{B}_{r_1}) + (1 - \theta)d(y, \mathcal{B}_{r_2}) \geq d(y, \mathcal{B}_{\theta r_1 + (1 - \theta)r_2})$$

which proves that $r \mapsto d(y, \mathcal{B}_r)$ is convex. \square